Gibbs Free Energy Perturbation Calculations: An Application to the Binding of Alkylammonium Cations by a Water-Soluble Calixarene

A. Ghoufi, C. Bonal, J. P. Morel, N. Morel-Desrosiers, and P. Malfreyt*

Laboratoire de Thermodynamique des Solutions et des Polymères, UMR CNRS 6003, Université Blaise Pascal (Clermont-Ferrand II), 24 avenue des Landais, 63177 Aubière Cedex, France

Received: March 31, 2004; In Final Form: May 26, 2004

We report results of calculations of the difference between the Gibbs free energies of association of the *p*-sulfonatocalix[4]arene with the tetramethylammonium and methylammonium cations in acidic aqueous solution. Good agreement is observed between the free energy difference predicted using our perturbation algorithm and the experimental value. We show the relative importance of the potential of mean force (pmf) bond correction and of the van der Waals and electrostatic contributions to the total change in the Gibbs free energy of complexation. We also provide a microscopic interpretation of these contributions to the total Gibbs free energy during the mutation process. In addition, we examine the hydration of the guest and the host as a function of the nature of the perturbation.

1. Introduction

Although the computation of free energy differences on molecular systems has been the subject of intense study during the past decade, the development of new algorithms and the study of more sophisticated biological systems still represent an area of active research. The traditional free energy perturbation (FEP)[1,2] and thermodynamic integration (TI)[2−4] methods are two of the most commonly used. These free energy calculation techniques have been successfully applied to the calculations of solubilities,[5] partition coefficients,[6] binding affinities in host−guest systems,[7−9] and free energies of solvation.[10−12] However, this kind of calculation cannot be considered as a systematic and routine job, especially when the perturbation between the two states A and B involves changes in the intramolecular (bond, valence angle, and dihedral angle potentials) and electrostatic interactions.

Recently, we used the microscopic and macroscopic approaches of molecular dynamics (MD) technique to study the association of the *p*-sulfonatocalix[4]arene with lanthanide, alkylammonium, and tetraalkylammonium cations[13] in aqueous solution. The MD simulations were fully consistent with the experimental thermodynamic data determined by microcalorimetry.[14,15] Whereas the binding of this ligand with alkylammonium cations is enthalpy-driven ($\Delta_r H° \ll 0$ and $T\Delta_r S° < 0$ or > 0), its binding with lanthanide cations is strongly entropy-driven ($\Delta_r H° > 0$ and $T\Delta_r S° \gg 0$). The MD simulations showed that the complexes formed with the tetraalkylammonium cations involve the inclusion of alkyl groups into the calixarene cavity, whereas the lanthanide cations are outside the cavity, in the vicinity of the sulfonate groups. The host and guest involved in the formation of an inclusion complex lose most of their degrees of freedom: this is accompanied by a strong entropy loss which masks the entropy gain due to the desolvation of the species upon binding, and as a result, the process is enthalpy-driven. We showed that it is the inclusion of the alkyl chains into the lipophilic cavity of the macrocyclic host that controls, through van der Waals interactions, the binding of the alkylammonium ions. On the other hand, we noticed that it is the partial desolvation of the metal cation and of the sulfonate groups of the calixarene, which are involved in ionic interactions, that explains the entropy-driven binding of the lanthanide cations. The calculated differences in the Gibbs free energies of complexation of lanthanide cations[13] showed excellent agreement with the experimental values.[14]

We deeply investigated the insertion of the tetramethylammonium, tetraethylammonium, and methylammonium cations into the calixarene cavity.[13,16] These MD simulations highlighted a correlation between the experimental $\Delta_r H°$ values and the number of atoms inserted into the cavity of the calixarene.[16] Furthermore, it was shown[16] that the specific behavior of Et_4N^+, which exhibits a remarkably negative enthalpy and entropy of binding,[14] results from the inclusion of the largest number of atoms into the cavity. These calculations are consistent with the thermodynamic properties determined from both microcalorimetry[14] and ^1H and ^{13}C NMR studies.[17] Two different models for the description of the alkylammonium cations were used. The first model represents explicitly the hydrogen atoms on the methyl group, whereas the second representation treats the CH_3 group as one interaction site. We showed that the structural properties of the complex and the energy contributions between the host and guest do not depend on the model used. These investigations were a necessary prerequisite for the present work.

In the present paper, we report the calculation of the difference between the Gibbs free energies of association of the *p*-sulfonatocalix[4]arene with the tetramethylammonium and methylammonium cations in acidic aqueous solution. The fact that the experimental value is available for comparison is an important point that allows us to carry out a deeper investigation of the different contributions to be incorporated in the statistical perturbation technique. In section 2, we present the functional form of the different potential energy functions and we briefly review the formalism of the thermodynamic perturbation theory. Section 3 contains the methodology used, the molecular details concerning the studied system, and the results of the calculations. We conclude in section 4 with a summary of the present results.

* Corresponding author. Patrice.MALFREYT@univ-bpclermont.fr.

10.1021/jp048598a CCC: $27.50
Published on Web 07/03/2004

2. Simulations

2.1. Potential Model. The *p*-sulfonatocalix[4]arene molecule is modeled using the all-atom version of the Cornell force field AMBER.[18] The overall potential function is of the form

$$U = U_{\text{bonds}} + U_{\text{angle}} + U_{\text{dihedral}} + U_{\text{vdw}} + U_{\text{ele}} \quad (1)$$

where

$$U_{\text{bonds}} = \sum_{\text{bonds}} \frac{1}{2} k_b (r - r_0)^2 \quad (2)$$

$$U_{\text{angle}} = \sum_{\text{angles}} \frac{1}{2} k_\theta (\theta - \theta_0)^2 \quad (3)$$

$$U_{\text{dihedral}} = \sum_{\text{dihedrals}} k_\phi [1 + \cos(n\phi + \delta)] \quad (4)$$

$$U_{\text{vdw}} = \sum_{i=1}^{N-1} \sum_{j>i}^{N} 4\epsilon_{ij} \left[\left(\frac{\sigma_{ij}}{r_{ij}} \right)^{12} - \left(\frac{\sigma_{ij}}{r_{ij}} \right)^{6} \right] \quad (5)$$

and where k_b, k_θ, and k_ϕ are the force constants for the deformation of bonds, angles, and dihedrals, respectively. The equilibrium values of bond distances and valence angles correspond to r_0 and θ_0, respectively. In the dihedral angle term, n is the periodicity and δ is the phase factor. The C−H and O−H covalent bonds are kept at a fixed length by using the SHAKE algorithm,[19] and the aromatic rings are kept planar by using six improper torsional potentials. In the AMBER force field, the nonbonded interactions between atoms separated by exactly three bonds (van der Waals 1−4 interactions) are reduced by a factor of 0.5 following ref 18. The bonds, bond angles, dihedral angles, and Lennard-Jones (LJ) parameters for the sulfonate group are taken from ref 20. The Lennard-Jones potential parameters for the interactions between unlike atoms are calculated by using the Lorentz−Berthelot mixing rules. We give below the equations relative to the electrostatic interactions in order to highlight the different contributions that are to be included in the perturbation calculations. In fact, the electrostatic energy using the Ewald sum method[21−23] for a neutral periodic system with an orthogonal axis is defined as

$$U_{\text{ele}} = U_{\text{real}} + U_{\text{reciprocal}} - U_{\text{self}} - U_{\text{excl}} \quad (6)$$

The real space term (U_{real}) is given by

$$U_{\text{real}} = \frac{1}{8\pi\epsilon_0} \sum_i \sum_a \sum_{j\neq i} \sum_b \left(\sum_{|n|=0}^{\infty} \frac{q_{ia} q_{ib}}{|r_{iajb} + n|} \text{erfc}(\alpha |r_{iajb} + n|) \right) \quad (7)$$

where the sums are over all atoms a in molecules i and all atoms b in molecules j. r_{iajb} is the distance between the atoms a and b belonging to the two different molecules i and j, and q_{ia} and q_{ib} represent the charges on atoms a and b, respectively. This term is pairwise-additive and short-ranged, and thus, a spherical cutoff can be used with periodic boundary conditions. α is chosen so that only atom−atom pair interactions between different molecules in the central cell ($n = 0$) need to be considered. erf(x) is the error function, whereas erfc(x) is the complementary error function. The reciprocal space term ($U_{\text{reciprocal}}$) is expressed as

$$U_{\text{reciprocal}} = \frac{1}{2V\epsilon_0} \sum_{k\neq 0} \frac{1}{k^2} \exp\left(-\frac{k^2}{4\alpha^2} \right) \left| \sum_i \sum_a q_{ia} \exp(ikr_{ia}) \right|^2 \quad (8)$$

where V is the simulation cell volume, r_{ia} is the Cartesian coordinate of site a in molecule i, and k is a reciprocal lattice vector defined as

$$k = 2\pi(l/L_x, m/L_y, n/L_z) \quad (9)$$

where l, m, and n take values 0, ±1, ±2, ... , ±∞. This term includes all the intramolecular interactions due to the bonded atoms. The additional term U_{excl} is added to correct for the contributions due to intramolecular electrostatic interactions. It is expressed as

$$U_{\text{excl}} = \frac{1}{8\pi\epsilon_0} \sum_i \sum_a \sum_{b\neq a} q_{ia} q_{ib} \frac{\text{erf}(\alpha r_{iaib})}{r_{iaib}} \quad (10)$$

where the sums are over the atoms bonded to atoms a and b of the same molecule i. A fourth correction term, U_{self}, is required to correct for the fact that the sum of Gaussian functions in the real space includes the interactions of each Gaussian with itself

$$U_{\text{self}} = \frac{\alpha}{4\pi^{3/2}\epsilon_0} \sum_i \sum_a q_{ia}^2 \quad (11)$$

An optional fifth term, U_{surf}, may be added in order to take into account the medium surrounding the sphere of simulation boxes. If the simulation boxes are embedded into a vacuum (with a relative permittivity of 1), the fifth term is given by the following expression[23,24]

$$U_{\text{surf}} = \frac{1}{6\epsilon_0 V} \left| \sum_i \sum_a q_{ia} r_{ia} \right|^2 \quad (12)$$

This term represents the dipole energy and has been already used in previous simulations of relatively simple systems.[25,26] This term must be carefully used if the simulated systems contain mobile ions. The fact that some ions can cross periodic boundary conditions may lead to discontinuous changes in the dipole moment of the cell and in the energy of the system. Additionally, in the AMBER force-field, the electrostatic interactions are treated using the traditional Ewald sum method with only the four terms described in (eq 6). To make our simulations consistent with previous simulations using this force field and involving molecules of biochemical and organic chemical interest, we do not take into account the U_{surf} contribution in the Ewald sum for both the production of configurations and the free energy calculations.

2.2. Free Energy Calculations. The difference in the Gibbs free energies (ΔG values) between molecular systems A and B are calculated with the free energy perturbation (FEP)[1,2] and thermodynamic integration (TI)[2−4] methods. In the FEP approach, the computation of the free energy difference between the two states A and B in the isothermal−isobaric constant-NpT ensemble is split into N_w intermediate contiguous states or windows defined by the coupling constant (λ)

$$\Delta G_{\text{FEP}} = G_B - G_A = \sum_{i=1}^{N_w} \Delta G(\lambda_i) = \sum_{\lambda=0}^{1} -RT \ln \left\langle \frac{V \exp\left[-\frac{(H(r;\lambda \pm \Delta\lambda) - H(r;\lambda))}{RT} \right]}{\langle V \rangle} \right\rangle_\lambda \quad (13)$$

where $H(r;\lambda)$ is the classical Hamiltonian corresponding to state

λ and depending only on the atomic coordinate set **r**. R is the molar gas constant, T is the absolute temperature, and V is the volume of the system. $\langle\,\rangle$ denotes an isothermal−isobaric ensemble average reflecting state λ. In our FEP simulations, the perturbations are performed in both directions ("double-wide sampling") with N_w windows over the entire simulation. The difference between the forward ($+\Delta\lambda$) and backward ($-\Delta\lambda$) simulations gives a lower-bound estimate of the error in the calculations.

The thermodynamic integration (TI) method expresses the change in free energy as the following integral

$$\Delta G_{TI} = \int_0^1 \left\langle \frac{\partial H(r;\lambda)}{\partial \lambda} \right\rangle_\lambda d\lambda \tag{14}$$

The derivative of $H(r;\lambda)$ with respect to λ is calculated as an average difference between $H(r;\lambda)$ and $H(r;\lambda \pm \delta\lambda)$

$$\left\langle \frac{\partial H(r;\lambda)}{\partial \lambda} \right\rangle_\lambda = \left\langle \frac{(H(r;\lambda \pm \delta\lambda) - H(r;\lambda)}{\delta\lambda} \right\rangle_\lambda \tag{15}$$

The finite difference integration thermodynamic (FDTI) method uses the perturbation formalism to calculate the derivative of the Hamiltonian with respect to λ as

$$\left\langle \frac{\partial H(r;\lambda)}{\partial \lambda} \right\rangle_\lambda = \frac{\partial G(\lambda)}{\partial \lambda} \simeq \frac{\Delta G(\lambda)}{\delta\lambda} = -\frac{RT}{\delta\lambda} \ln \left\langle \frac{V \exp\left[-\frac{(H(r;\lambda \pm \delta\lambda) - H(r;\lambda))}{RT} \right]}{\langle V \rangle} \right\rangle \tag{16}$$

The change in the Gibbs free energy (ΔG_{FDTI}) is thus expressed as the integral of $\langle(\partial H(r;\lambda)/\partial\lambda)\rangle_\lambda$ calculated using eq 16. $\delta\lambda$ is taken sufficiently small ($\delta\lambda = 0.001$) to avoid hysteresis between calculations carried out from state λ to state ($\lambda + \delta\lambda$) and from state λ to state ($\lambda - \delta\lambda$). Simulations in the forward ($+\delta\lambda$) and backward ($-\delta\lambda$) directions provide the average value of the derivative with an estimate of the statistical uncertainty. The integration over λ (eq 14) is carried out either by a trapezoidal algorithm or by fitting the integrand as a function of λ and integrating it analytically.

The variations of the Hamiltonian $H(r;\lambda)$ are calculated using a linear combination of the LJ parameters (σ and ϵ) of the initial state A ($\lambda = 0$) and the final state B ($\lambda = 1$) using the following mixing rules:

$$\epsilon_{ij}(\lambda) = \lambda\left(\sqrt{\epsilon_{ii}(1)\epsilon_{jj}}\right) + (1-\lambda)\left(\sqrt{\epsilon_{ii}(0)\epsilon_{jj}}\right) \tag{17}$$

$$\sigma_{ij}(\lambda) = \lambda\left(\frac{\sigma_{ii}(1)+\sigma_{jj}}{2}\right) + (1-\lambda)\left(\frac{\sigma_{ii}(0)+\sigma_{jj}}{2}\right) \tag{18}$$

where i and j represent perturbed and unperturbed atom types, respectively.

The atomic site mass (m) and the atomic site charge (q) are also expressed as a function of λ as follows

$$q_i(\lambda) = \lambda q_i(1) + (1-\lambda) q_i(0) \tag{19}$$

$$m_i(\lambda) = \lambda m_i(1) + (1-\lambda) m_i(0) \tag{20}$$

where i represents the perturbed atomic site.

2.3. Computational Methodology. The system consists either of a *p*-sulfonatocalix[4]arene molecule bound to an alkylammonium cation in 900 water molecules or an alkylammonium cation alone in 500 water molecules. In the first case, three Na^+ ions are added to ensure neutral charge in the simulation box, whereas in the second case, only one Cl^- ion is added. The water molecules are represented by the TIP3P model.[27] In acidic solution at pH 2, all the phenolic hydroxy groups are protonated according to the pK_a values.[28−30] The sodium ions are located in such a way that the $Na^+ \cdots Na^+$ and $Na^+ \cdots$calixarene distances are larger than the cutoff radius. We check that these distance criteria are satisfied during the different perturbation calculations. The starting configuration of the complex with the tetramethylammonium cation is the equilibrium configuration arrived at in the previous MD calculation.[16] The periodic boundary conditions are applied in the three dimensions. The Ewald summation technique is applied for the treatment of the long-range electrostatic interactions[31] with the range of the real space interaction controlled by the convergence parameter $\alpha = 0.2651$ within a relative error of 10^{-6}. The reciprocal space summation is thus performed using either $k_{max} = \{8 \times 8 \times 8\}$ for the alkylammonium cation in the complex or $k_{max} = \{7 \times 7 \times 7\}$ for the free cation in solution. The equations of motion are integrated using the Verlet Leapfrog algorithm scheme in the NpT ensemble ($p = 1$ atm and $T = 298$ K) with a 2 fs time step. We use the Berendsen algorithm[32] with coupling constants of 0.1 ps (temperature) and 0.5 ps (pressure). We use the multiple time step algorithm[33] in conjunction with the Verlet neighbor list. The interval for computing the secondary force is taken equal to five steps with a large cutoff ($r_c = 12$ Å), whereas the primary force is calculated every time step within a cutoff of 8 Å. The Verlet list sphere radius is fixed to 14 Å. Using this set of parameters, we check that the total energy of our systems is well conserved with deviations <0.3%. The atomic charges on the calixarene anion are fitted to reproduce the molecular electrostatic potential created around the uncomplexed calixarene at the HF level with a 6-31G basis set on a number of potential energy surfaces, generated from 1.4, 1.6, 1.8, and 2.0 times the van der Waals atomic radii. We use the CHELPG[34] procedure as a grid-based method. The quantum ab initio calculations are carried out using the GAMESS package.[35] The partial charges on the NH_4^+ and $MeNH_3^+$ cations, reported in Table 1, have been taken from ref 37 and have been calculated using the 6-31G* basis. The configurations are generated using the DL_POLY_ MD package.[36]

TABLE 1: Bond Lengths, Bond Angles, and Nonbonded Interaction Parameters Reported with the Atomic Charges for Me_4N^+ and $MeNH_3^+$ [37]

bond		r_0 (Å)	
N_T-C_{3T}		1.471	
$N-C_3$		1.471	
$N-H$		1.010	
angle bending parameters		k_θ (kJ mol^{-1} rad^{-2})	θ_0 (deg)
$C_{3T}-N_T-C_{3T}$		418.4	109.5
C_3-N-H		418.4	109.5
$H-N-H$		418.4	109.5
atom type	q (e)	σ (Å)	ϵ (kJ mol^{-1})
C_{3T}	0.250	3.960	0.607
C_3	0.310	3.775	0.867
N_T	0.000	3.250	0.711
N	−0.300	3.250	0.711
H	0.330	0.000	0.000

3. Results and Discussions

The difference between the Gibbs free energies of binding of the *p*-sulfonatocalix[4]arene with $MeNH_3^+$ and Me_4N^+ in water is calculated following the thermodynamic cycle given

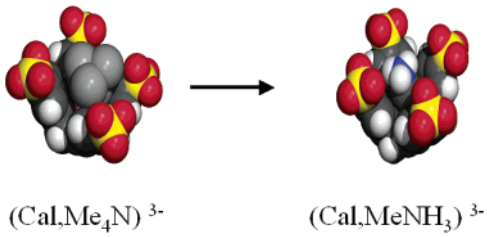

Figure 1. Snapshots of the complexes of the *p*-sulfonatocalix[4]arene with Me_4N^+ and $MeNH_3^+$ cations (Cal stands for calixarene).

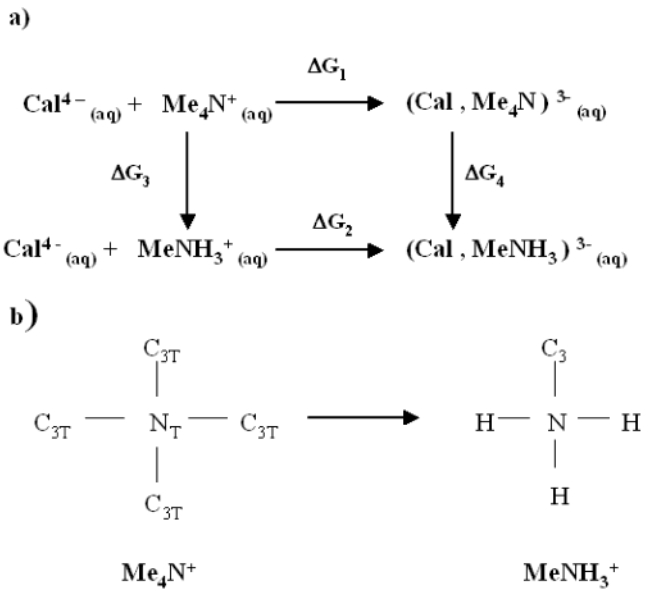

Figure 2. (a) Thermodynamic cycle used to determine the relative Gibbs free energy of complexation ($\Delta\Delta G_c$) defined as $\Delta\Delta G_c = \Delta G_1 - \Delta G_2 = \Delta G_3 - \Delta G_4$ (Cal^{4-} stands for the *p*-sulfonatocalix[4]arene in acidic aqueous medium). (b) Schematic diagram showing the transformation of Me_4N^+ into $MeNH_3^+$. The symbols C_{3T} and C_3 represent methyl groups, whereas N and N_T represent nitrogen atoms. The symbol H corresponds to the hydrogen atom.

in Figure 2a, which involves the mutation of Me_4N^+ into $MeNH_3^+$. The difference between the experimental Gibbs free energies of binding, $\Delta G_1 - \Delta G_2$, is equal to the computed difference, $\Delta G_3 - \Delta G_4$. ΔG_1 and ΔG_2, which have been determined by microcalorimetry,[14] are equal to −25.1 and −15.1 kJ mol^{-1}, respectively. ΔG_4 is calculated by the mutation of complexed Me_4N^+ into complexed $MeNH_3^+$, whereas ΔG_3 corresponds to the mutation of free Me_4N^+ into free $MeNH_3^+$. The Me_4N^+ cation is modeled as a five center molecule using a united atom (UA) description of the CH_3 groups. The methyl group of the $MeNH_3^+$ cation is also described with the UA model (Figure 2b). The equilibrium bond lengths, bond angle parameters, and nonbonded parameters are taken from ref 37 and are listed in Table 1. The angle bending parameters are similar for the three internal angles, and the bond lengths are kept fixed at their equilibrium values using the SHAKE algorithm. The structure and the UA description of the $MeNH_3^+$ and Me_4N^+ cations do not involve intramolecular nonbonded interaction; the rigidity of the chemical bonds and the equivalence between the valence angle parameters for the two ions imply that mutation of free Me_4N^+ into free $MeNH_3^+$ in the gas phase would yield a Gibbs free energy contribution equal to zero. This particularity implies that the computed value ΔG_3 is equal to the difference between the Gibbs free energies of hydration of the two ions. This allows an additional check of our calculations. The mutation of Me_4N^+ into $MeNH_3^+$ is shown schematically in Figure 2b and is achieved by transforming three methyl groups (C_{3T}'s) into three H atoms, one methyl group (C_{3T}) into another methyl group (C_3), and the nitrogen atom (N_T) into N. The transformation is performed using three separate stages.

The first stage consists of calculating the contribution to the total Gibbs free energy due to the change of the N_T-C_{3T} bond length of 1.471 Å into the N_T-H bond length of 1.010 Å. In this stage, the bond length is changed but the chemical nature of the C_{3T} atom is unchanged. Pearlman and Kollman[38] have shown the necessity to take into account the contribution of chemical bonds whose equilibrium lengths are changing during the perturbation process. This contribution, called ΔG_{bond}, is far from being negligible and is referred to as a potential of mean force (pmf) correction along the perturbed bonds. The value of the equilibrium bond length (r_0) becomes a function of λ and varies according to the following relationship:

$$r_0(\lambda) = \lambda r_0(1) + (1 - \lambda) r_0(0) \tag{21}$$

The difference in $[H(r; r_0(\lambda \pm \Delta\lambda)) - H(r; r_0(\lambda))]$ is calculated from the Me_4N^+ topology by stretching/shrinking each constrained N_T-C_{3T} bond along its length ($r_0(\lambda)$) and moving each atom along the bond vector. The calculation of the ΔG_{bond} term includes the energetic contributions of U_{vdw}, U_{real}, $U_{reciprocal}$, and U_{excl} defined above. This pmf bond correction is calculated over 11 windows. Each of them consists of 10 ps of equilibration and 20 ps of acquisition corresponding to 2000 configurations for the production phase. The total time, for the calculation of ΔG_{bond}, is then 880 ps.

The second stage involves the change in the van der Waals parameters when going from the Me_4N^+ to the $MeNH_3^+$ topology with chemical bond lengths corresponding to the $MeNH_3^+$ structure. This mutation gives a ΔG_{vdw} contribution. This part of the total Gibbs free energy involves only the calculation of the difference in the van der Waals contributions (U_{vdw} values). This perturbation process is divided into 21 windows with 10 ps of equilibration followed by 20 ps of data collection. The time for the transformation of the nonbonded parameters is thus 1260 ps.

In the last stage, the charges are mutated in the $MeNH_3^+$ topology for the five atoms according to the atomic charges given in Table 1. The electrostatic contribution ΔG_{ele} is calculated using the U_{real}, $U_{reciprocal}$, U_{excl}, and U_{self} parts of the Ewald sum method over 11 windows. The time span for the electrostatic interaction is increased; the system is equilibrated during a period of 10 ps, and the averages are carried out over 50 ps for each window. The total time for the electrostatic contribution is 1320 ps. This means that the full mutation of Me_4N^+ into $MeNH_3^+$ requires a simulation time of 3.24 ns.

To ascertain the accuracy of our developed algorithms, we have monitored in Figure 3 the different contributions to $\Delta G(\lambda)$ for the free cation and to $(\partial H(r; \lambda)/\partial\lambda)$ for the complexed cation as a function of the simulation time for a given λ. We define the point of convergence as the point where additional sampling does not change the result. We check that the convergence is reached after 20 ps and occurs roughly at the same time for the individual terms ΔG_{bond}, ΔG_{vdw}, and ΔG_{ele} for both $\Delta G(\lambda)$ and the free energy derivative of the TI simulations. Obviously, the simulation time for each window and each type of mutation is appropriate for the calculation of the total Gibbs free energy difference.

Figure 4 shows the three contributions to the computed changes in Gibbs free energy as a function of the coupling parameter. Part a of Figure 4 shows that ΔG_{bond} and ΔG_{ele} for the free cation in water decrease linearly with λ, whereas ΔG_{vdw}

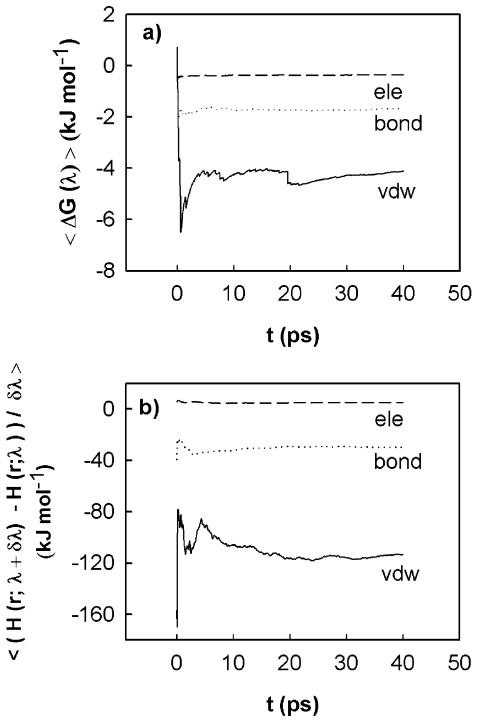

Figure 3. (a) Accumulated Gibbs free energy change averages ($\Delta G(\lambda)$ values) vs time for the mutation of free Me_4N^+ into free $MeNH_3^+$ in water for $\lambda = 0.2$. (b) Free energy derivative averages calculated using TI formalism as a function of time for the complexed cations at $\lambda = 0.4$ for the following changes: transformation of the bond lengths (····), mutation of the van der Waals parameters (—), and mutation of the atomic charges (– – –).

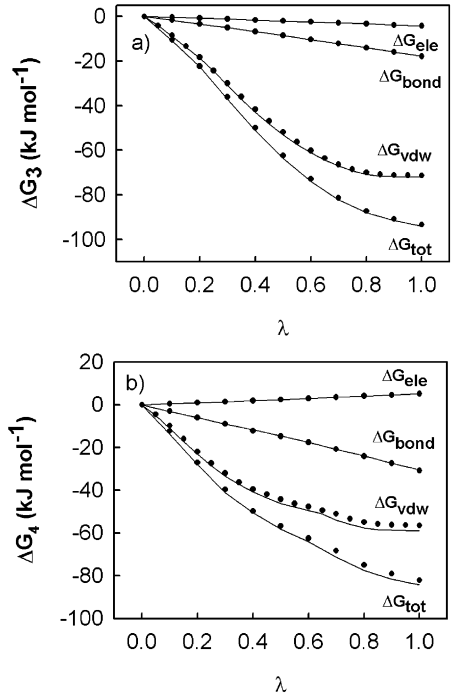

Figure 4. Computed Gibbs free energy changes ΔG_{bond}, ΔG_{vdw}, ΔG_{ele}, and ΔG_{tot} as a function of the coupling parameter (λ) in forward (—) and backward (●) processes for the mutations of the (a) free and (b) complexed cations.

decreases linearly up to 0.6 and then remains constant. The corresponding total Gibbs free energy values are reported in Table 2. Concerning the mutation of the free cations in solution, we observe that the major contribution to the total Gibbs free energy comes from the van der Waals contribution. We also note that the pmf bond correction represents 19% of ΔG_{total}, which shows that the contributions of the intraperturbed interactions to the free energy are far from being negligible. The comparison between the computed difference in the Gibbs free energies of hydration of Me_4N^+ and $MeNH_3^+$ and the corresponding values available in the literature[39,40] is very satisfactory in view of the range of the data.

TABLE 2: Different Contributions to the Total Gibbs Free Energy Change Reported for Both the Uncomplexed Cation (ΔG_3) and the Complexed Cation (ΔG_4)[a]

	ΔG_{bond} (kJ mol^{-1})	ΔG_{vdw} (kJ mol^{-1})	ΔG_{ele} (kJ mol^{-1})	ΔG_{tot} (kJ mol^{-1})
		$Me_4N^+ \rightarrow MeNH_3^+$		
$\Delta G_{3,FEP}$	-17.8_5	-71.5_8	-4.22_4	-93.5_8
$\Delta G_{3,TI}$	-17.8_9	-72.4_9	-4.22_4	-94.4_9
$\Delta G_{3,FDTI}$	-17.8_5	-73.2_9	-4.22_4	-95.2_9
ΔG°_{hyd}				-87.9; -100.0[39,40]
		$(Cal,Me_4N)^{3-} \rightarrow (Cal, MeNH_3)^{3-}$		
$\Delta G_{4,FEP}$	-30.1_9	-57.7_{12}	5.1_5	-82.7_{12}
$\Delta G_{4,TI}$	-30.5_5	-58.6_{12}	5.1_5	-84.0_{12}
$\Delta G_{4,FDTI}$	-30.5_5	-58.2_{12}	5.1_5	-83.6_{12}
$\Delta\Delta G_{c,FEP}$				-10.8_{12}
$\Delta\Delta G_{c,TI}$				-10.4_{12}
$\Delta\Delta G_{c,FDTI}$				-11.6_{12}
$\Delta\Delta G^\circ_{c,exp}$				-10.0_4

[a] The differences in the computed and experimental Gibbs free energies of complexation ($\Delta\Delta G_c$) are also given. The subscript indicates the accuracy of the last decimal(s). The number -17.8_5 means -17.8 ± 0.5.

To further analyze the negative ΔG_{vdw} contribution, we study the structure and the water−cation energy contribution as a function of the nature of the perturbation. Figure 5a shows the alkylammonium N−O_w radial distribution functions (rdf's) for different types of mutations, where O_w denotes the oxygen atom of water molecules. The major changes in the shape of the radial distribution functions occur during the van der Waals perturbation process, with the coordination number decreasing from 20 to 6. The position of the first shell shows the evolution from a broad peak located at $r = 4.8$ Å to a well defined peak at $r = 2.8$ Å. This means that the van der Waals mutation involves a change from a hydrophobic solute to a tightly bound water structure. The distribution of the angle formed between the water dipole vector and the N−O_w distance vector, shown in part b of Figure 5, is almost flat for Me_4N^+, with a broad peak corresponding to a range of angles between 70 and 80°. This suggests a tangential orientation of water molecules around the solute. The change in the van der Waals interactions leads to a reorientation and a structuring of the water molecules in the first hydration shell of the solute with a peak at $\cos\theta = 1$, indicating that the oxygen atoms of the water molecules point toward the nitrogen atom of the cation. This orientation is thus favorable for optimal hydrogen bonds between the solute and water molecules. Part c of Figure 5 presents the number of hydrogen bonds as a function of the coupling parameter. We consider that a hydrogen bond can be formed between a water molecule and the solute if the distance between the nitrogen atom of the cation and an oxygen atom of a water molecule is <3.5 Å and the distance between a hydrogen atom of the cation and an oxygen atom of a water molecule is <2.45 Å. We observe an increase of the number of hydrogen bonds from 0 to 3.7 during the van der Waals mutation. Our simulations provide the same number of hydrogen bonds for the methylammonium cation as that calculated by Jorgensen and Gao.[37] The inset of Figure 5c shows that the $O_w-H_{cation}-H_w$ angular distribution, for water molecules satisfying the distance criteria

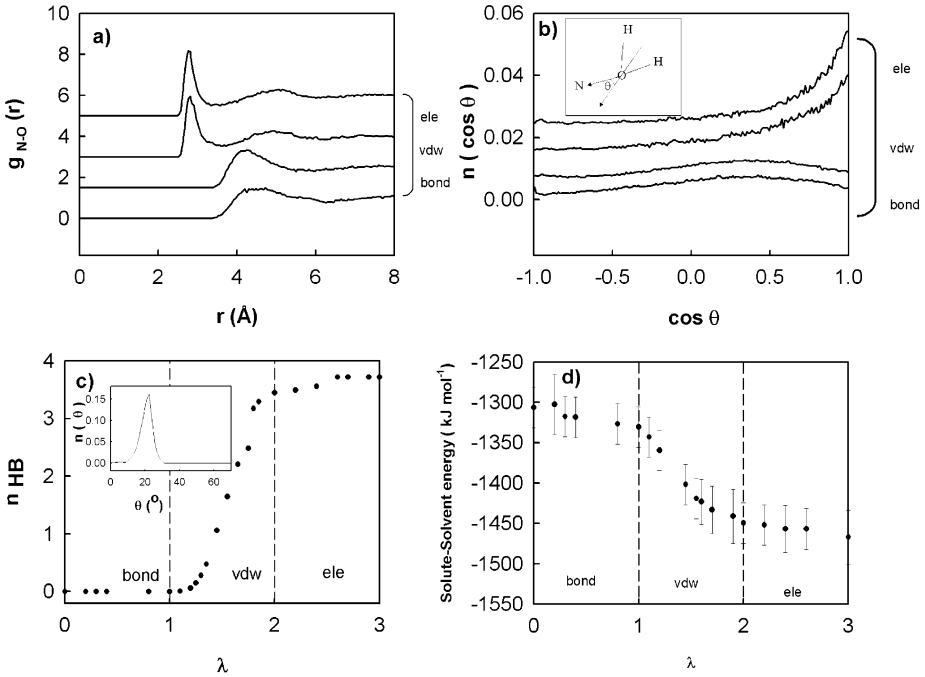

Figure 5. (a) Computed alkylammonium N−O_w radial distribution functions (O_w denotes the oxygen atom of water molecules). (b) Angular distribution of the angle between the dipole vector of the water molecules and the O_w−N distance vector. (c) Number of hydrogen bonds between the cation and the water molecules and angular distribution function of the O_w−H_{cation}−H_w angle for water molecules forming hydrogen bonds with the cation. (d) Solute−solvent interaction energy (kJ mol^{-1}) as a function of the type of transformation.

for the formation of hydrogen bonds, presents a well pronounced peak at about $\theta = 20°$. We check that this angle is always $<30°$ when the two distance criteria are satisfied.[41,42] The intermolecular energy between the alkylammonium cations and the solvent molecules are displayed in Figure 5d as a function of the mutation process and are calculated by including the nonbonded interactions and the four terms of the Ewald sum. The transformations of the bond lengths and atomic charges lead to decreases in the solute−solvent energy of 24 and 17 kJ mol^{-1}, respectively. The decrease reaches 119 kJ mol^{-1} at the end of the van der Waals mutation process. This clearly shows that the dominant negative ΔG_{vdw} contribution to the total free energy change is associated with the hydration of the cation. The mutation of the methyl groups into hydrogen atoms leads to the formation of hydrogen bonds with a strong structuration of the first hydration shell and results in a decreasing negative solute−solvent interaction energy during the van der Waals process.

Concerning the mutation of (Cal, Me_4N)$^{3-}$ into (Cal, $MeNH_3$)$^{3-}$, we mutate the most deeply inserted methyl group of Me_4N^+ into the methyl group of $MeNH_3^+$. The three remaining methyl groups, which are located toward the upper rim, are transformed into hydrogen atoms. This is done in order to be consistent with the previous MD simulation[16] of (Cal, $MeNH_3$)$^{3-}$ which has shown that the methyl group is deeply located in the calixarene cavity, whereas the hydrogen atoms are located toward the upper rim of the calixarene and point toward the water molecules.

We observe in part b of Figure 4 some changes in the variations with respect to the λ values of the three contributions observed upon mutation of the complexed cation compared to those observed for the mutation of the free cation (Figure 4a). ΔG_{ele} and ΔG_{bond} still vary linearly with λ. However, the electrostatic contribution now increases, whereas the bond contribution decreases with a slope larger than that for the free cation. ΔG_{vdw} decreases continuously up to 0.4 with a resulting total value smaller than that calculated for the free cations. The total values of the three contributions are given in Table 2 as a function of the formalism used. The FEP, TI, and FDTI methods yield similar results within the range of the standard deviations. We notice that the bond contribution reaches 36% of the total value. This interesting result means that making the usual assumption that the bond contribution cancels between the mutations of the free cations and complexed cations during the thermodynamic cycle would lead to erroneous values in the difference in the Gibbs free energy of association. The relative importance of the intraperturbed contributions has already been underlined by Kollman et al.[38] Table 2 shows excellent agreement between the differences in the computed and experimental Gibbs free energies of complexation with a maximal relative error of 13% for the FDTI technique.

Further work is needed to clarify what exactly occurs at the microscopic level to explain the change in sign of the electrostatic contribution. The integration of the distributions of the distance between the centers of mass (com's) of the hydroxy phenolic groups and the alkylammonium cation shows that the distance corresponding to the unit value of the integrals decreases during the mutations with a more pronounced trend during the van der Waals mutation (Figure 6a). We also observe in Figure 6a an opposite trend for the integration of the distance between the com's of the sulfonate groups and the alkylammonium cation. The distance corresponding to the unit value of the integral increases during the mutation process with also a more marked change during the van der Waals process. In fact, we see a decrease in the distance between the cation and the com of the lower rim and an increase of the distance between the cation and the upper rim. These results suggest a slightly deeper insertion into the cavity of the calixarene for $MeNH_3^+$. The distribution of the angle (Figure 6e) formed between the centers of mass of the sulfonate groups, of the cation, and of the hydroxy groups shows that an important change occurs during the mutation of the nonbonded parameters. The distribution for the Me_4N^+ topology, shown in Figure 6b, corresponds to a well defined peak at 180°, indicating that the cation is

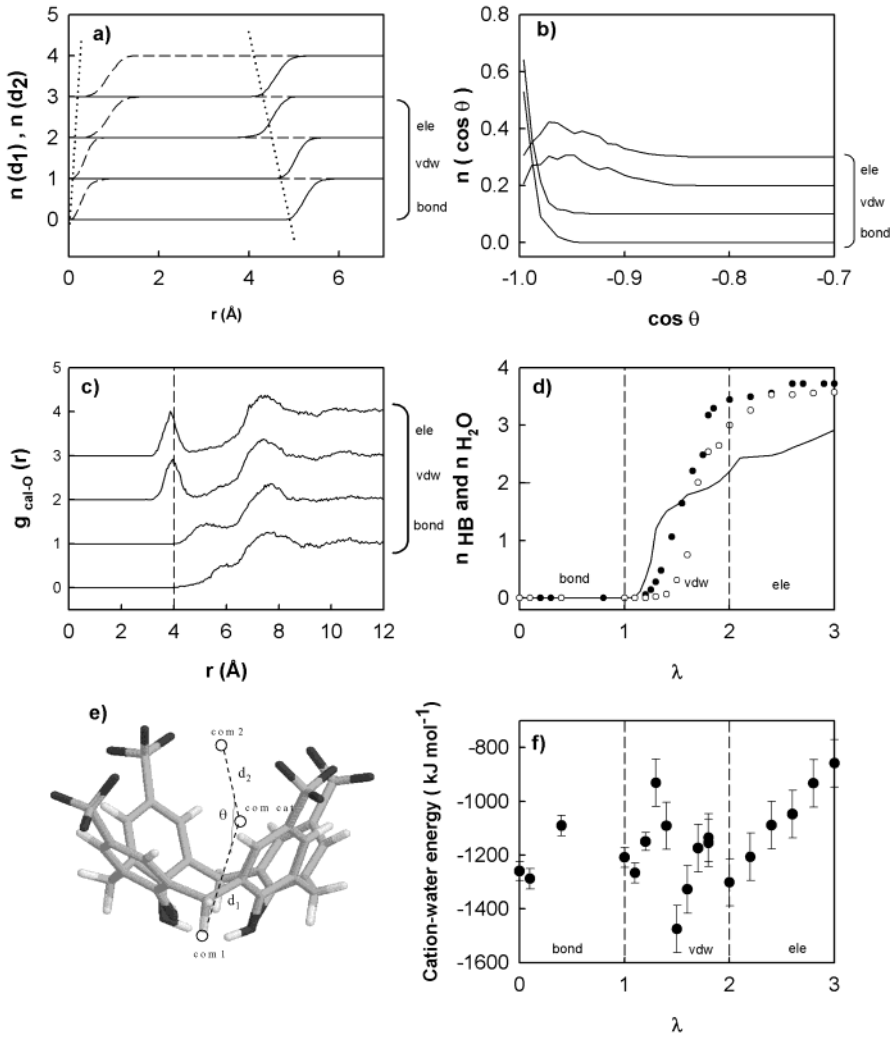

Figure 6. (a) Integration of the distributions of the distance between the alkylammonium cation com and the phenolic hydroxy groups com (—) and of the distributions of the distance between the cation com and the sulfonate groups com (– – –). The dotted lines are used as a guide for the eye. (b) Angular distribution of the θ angle, defined in part e of this figure as a function of the type of mutation. (c) Calixarene com−water com rdf's as a function of the transformation. (d) The solid line represents the number of water molecules located in the cavity of the calixarene, whereas the dots correspond to the number of hydrogen bonds formed between the water molecules and the free (●) and complexed (○) cations. (e) Schematic representation showing the centers of mass of the hydroxy groups (com1), of the sulfonate groups (com2), and of the cation (com cat). (f) Cation−water energy (kJ mol^{-1}) as a function of the mutation.

located symmetrically inside the cavity with little degrees of freedom. For $MeNH_3^+$, the distribution is broader, with a maximum located between 150 and 160° underlining a larger sampling of the cavity for this topology (Figure 6b). Concerning the solvation of the cavity of the calixarene, we have plotted, in part c of Figure 6, the calixarene com−water com radial distribution functions. We showed in a previous study[13] that the cavity of the calixarene can be assimilated to a sphere with a radius of ∼5 Å. We take a limit value of 4 Å to ensure that we are really inside the cavity. Figure 6c shows that some water molecules penetrate inside the cavity during the van der Waals mutation, with the number of water molecules increasing from 0 to 2.9 during the total mutation (Figure 6d). We see that the transformation of the guest from Me_4N^+ to $MeNH_3^+$ involves a more important hydration of the upper part of the cavity. The analysis of the cation−water interaction energy in Figure 6f is difficult due to large standard deviations. The order of magnitude of these fluctuations is similar to the difference in the cation−water energies calculated during the van der Waals mutation of the free cations and does not allow a detailed microscopic interpretation during the van der Waals transformation. However, a significant linear increase in the cation−water energy is found during the transformation of the charges. The number of hydrogen bonds calculated both for the free and complexed cation as a function of the type of transformation, displayed in part d of Figure 6, does not show significant variations between the two situations.

This allows us to extract from our simulations a more detailed picture of the first and second hydration shell of the alkylammonium cation. Part a of Figure 7 shows the N−O_w radial distribution function at the end of the transformation of the charges for the free and complexed cation. The angular distribution of the angle between the dipole vector of the water molecules and the O_w−N position vector in the first hydration shell shows a peak displaced from cos $\theta = 1$ to cos $\theta = 0.44$ (Figure 7b). This means that the number of water molecules in the first hydration shell is unchanged by the presence of the calixarene, whereas the orientation of the water molecules changes around the complexed cation. However, these distributions show that the oxygen atoms of the water molecules in the first hydration shell point toward the cation. As seen in Figure 7b, the distribution of the same angle with the water molecules in the second coordination shell shows a flat profile, indicating no preferential orientation for the water molecules around the

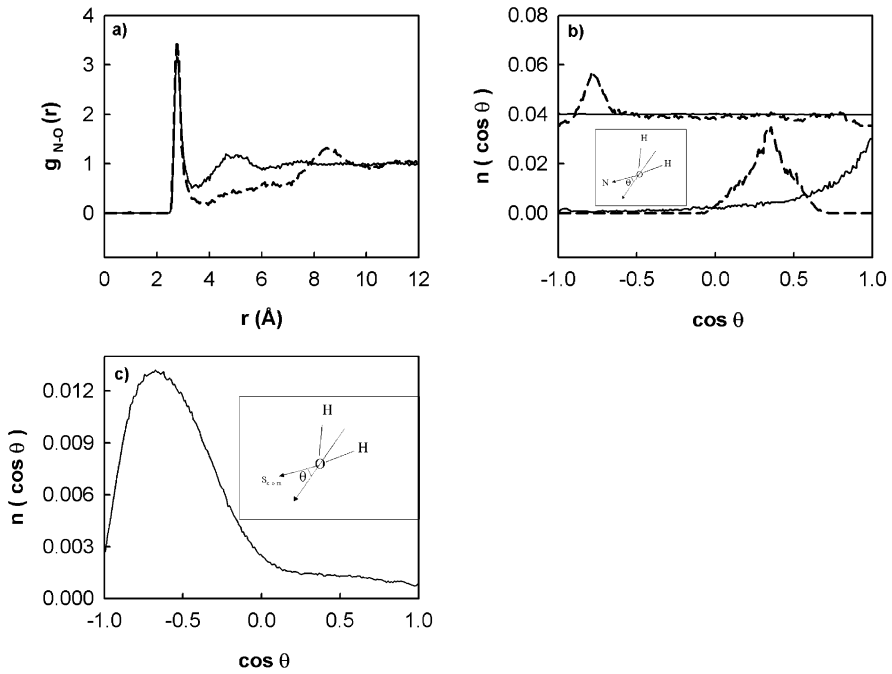

Figure 7. (a) N ($MeNH_3^+$)−O_w rdf's for the free (—) and complexed (− − −) cation at the end of the mutations of the atomic charges. (b) Angular distribution of the angle between the dipole vector of water molecules and the oxygen−nitrogen distance vector in the first hydration shell for the free (—) and complexed (− − −) cations. (distributions corresponding to the second hydration shell are offset by 0.035 units for clarity). (c) Angular distribution of the angle between the dipole vector of water molecules and the water O_w−SO_3^- com distance vector in the first hydration shell for complexed $MeNH_3^+$.

free cation. This distribution calculated in the complex exhibits a peak close to cos $\theta = -0.8$. This change of sign for this distribution means that the water molecules of the second hydration shell are now oriented with the hydrogen atoms pointing toward the hydrogen atoms of $MeNH_3^+$. This structural change makes positive electrostatic contributions. It may be explained by the presence of sulfonate groups which perturb the structure of the second hydration shell of the cation. Interestingly, the distribution of the angle between the dipole vector of the water molecules and the O_w−SO_3^- com distance vector, shown in Figure 7c, presents a peak located at about the same point (cos $\theta = -0.75$). This seems to support the conclusion that the second hydration shell of the cation is constituted by water molecules which also give hydrogen bonds with the sulfonate groups. These hydrogen bonds with the sulfonate groups imply a preferential orientation with the hydrogen atoms pointing toward the sulfonate groups and explain why these hydrogen atoms are now directed toward the hydrogen atoms of $MeNH_3^+$. The gradual increase of the charges may explain the increase in the corresponding cation−solvent interaction energy and the resulting positive value in the change in the ΔG_{ele} contribution.

4. Conclusions

We report calculations in the changes in the Gibbs free energies of association of the *p*-sulfonatocalix[4]arene complexes with Me_4N^+ and $MeNH_3^+$ in water at pH 2. This kind of simulation intends to decouple the different mutations from the intial state to the final state into three stages. The first stage consists of changing the bond lengths. The second stage changes the Lennard-Jones parameters, whereas the last one mutates the atomic charges. We have developed specific perturbation algorithms based on the FEP, TI, and FDTI methods and underlined the different contributions of the Ewald sum method to be taken into account in the pertubation calculations.

Our results underline that it is necessary to consider the changes in the bond lengths during a change in the topology and that this contribution does not cancel during the thermodynamic cycle. This contribution, which is essentially a potential of mean force correction, represents a nonnegligible part of the total value; this has been evidenced from the calculations of the change in the Gibbs free energy of hydration of free Me_4N^+ and $MeNH_3^+$ and of the change in the corresponding Gibbs free energy of complexation with the calixarene. Our calculations show excellent agreement between the computed and experimental relative values of the Gibbs free energy of complexation within a maximal deviation of 13%.

We have proposed a microscopic interpretation of the negative van der Waals contribution to the change in the free energy of hydration for the mutation of free Me_4N^+ into free $MeNH_3^+$ by analyzing the evolution of the formation of hydrogen bonds during the different transformations. We have also closely examined the positive value of the electrostatic contribution during the mutation of complexed Me_4N^+ into complexed $MeNH_3^+$. We have explained this positive contribution by changes in the orientational distributions of the water molecules in the second hydration shell of the complexed cation; this structuring of the second hydration shell of $MeNH_3^+$ is due to the formation of hydrogen bonds between these water molecules and the sulfonate groups.

References and Notes

(1) Zwanzig, R. W. *J. Chem. Phys.* **1954**, *22*, 1420.
(2) Mezei, M.; Beveridge, D. L. *Ann. N.Y. Acad. Sci.* **1986**, *482*, 1.
(3) Pearlman, D. A. *J. Comput. Chem.* **1994**, *15*, 105.
(4) Mezei, M.; Swaminathan, S.; Beveridge, D. L. *J. Am. Chem. Soc.* **1978**, *100*, 3255.
(5) Swope, W. C.; Andersen, H. C. *J. Phys. Chem.* **1984**, *88*, 6548.
(6) Jorgensen, W. L. Free Energy Changes in Solution. In *Encyclopedia of Computational Chemistry*; Schleyer, P. v. R., Ed.; Wiley: New York, 1998; Vol. 2, pp 1061−1070.
(7) Lamb, M. L.; Jorgensen, W. L. *Curr. Opin. Chem. Biol.* **1997**, *1*, 449.

(8) Jorgensen, W. L.; Duffy, E. M.; Essex, J. W.; Severance, D. L.; Blake, J. F.; Jones-Hertzog, D. K.; Lamb, M. L.; Tirado-Rives, J. In *Biomolecular Structure and Dynamics*; Vergoten, G., Theophanides, T., Eds.; Kluwer: Amsterdam, The Netherlands, 1997; pp 21−34.

(9) Bohm, H. J.; Klebe, G. *Angew. Chem., Int. Ed. Engl.* **1996**, *35*, 2588.

(10) Buckner, J. K.; Jorgensen, W. L. *J. Am. Chem. Soc.* **1989**, *111*, 2507.

(11) Rao, B. G.; Singh, U. C. *J. Am. Chem. Soc.* **1989**, *111*, 3125.

(12) Rizzo, R. C.; Jorgensen, W. L. *J. Am. Chem. Soc.* **1999**, *121*, 4827.

(13) Mendes, A.; Bonal, C.; Morel-Desrosiers, N.; Morel, J. P.; Malfreyt, P. *J. Phys. Chem. B* **2002**, *106*, 4516.

(14) Bonal, C.; Israeli, Y.; Morel, J. P.; Morel-Desrosiers, N. *J. Chem. Soc., Perkin Trans. 2* **2001**, 1075.

(15) Perret, F.; Morel, J. P.; Morel-Desrosiers, N. *Supramol. Chem.* **2003**, *15*, 199.

(16) Ghoufi, A.; Bonal, C.; Morel, J. P.; Morel-Desrosiers, N.; Malfreyt, P. *J. Phys. Chem. B* **2004**, *108*, 5095.

(17) Lehn, J. M.; Meric, R.; Vigneron, J. P.; Cesario, M.; Guilhem, J.; Pascard, C.; Asfari, Z.; Vicens, J. *Supramol. Chem.* **1995**, *5*, 97.

(18) Cornell, W. D.; Cieplak, P.; Bayly, C. I.; Gould, I. R.; Merz, K. M., Jr.; Ferguson, D. M.; Spellmeyer, D. M.; Fox, T.; Caldwell, J. W.; Kollman, P. *J. Am. Chem. Soc.* **1995**, *117*, 5179.

(19) Ryckaert, J. P.; Ciccotti, G.; Berendsen, H. J. C. *J. Comput. Phys.* **1977**, *23*, 327.

(20) Tobias, D. J.; Klein, M. L. *J. Phys. Chem.* **1996**, *100*, 6637.

(21) Nosé, S.; Klein, M. L. *Mol. Phys.* **1983**, *50*, 1055.

(22) Nosé, S.; Klein, M. L. In *Simulation of Liquids and Solids*; Ciccotti, G., Frenkel, D., McDonald, I. R., Eds.; North-Holland: Amsterdam, The Netherlands, 1987.

(23) de Leeuw, S. W.; Perram, J. W.; Smith E. R. *Proc. R. Soc. London, Ser. A* **1990**, *373*, 27.

(24) Deem, M.; Newsam, J.; Sinha, S. *J. Phys. Chem.* **1990**, *94*, 8356.

(25) Perera, L.; Essmann, U.; Berkowitz, M. L. *J. Chem. Phys.* **1995**, *102*, 450.

(26) Boulougouris, G.; Economou, I. G.; Theodorou, D. N. *J. Phys. Chem. B* **1998**, *102*, 1029.

(27) Jorgensen, W. L.; Chandrasekhar, J.; Madura, J. D. *J. Chem. Phys.* **1983**, *79*, 926.

(28) Scharff, J. P.; Mahjoubi, M.; Perrin, R. *New. J. Chem.* **1991**, *15*, 883.

(29) Arena, G.; Cali, R.; Lombardo, G. G.; Rizzarelli, E.; Sciotto, D.; Ungaro, R.; Casnati, A. *Supramol. Chem.* **1992**, *1*, 19.

(30) Yoshida, I.; Yamamoto, N.; Sagara, F.; Ishii, D.; Ueno, D.; Shinkai, S. *Bull. Chem. Soc. Jpn*. **1992**, *65*, 1012.

(31) Allen, M. P.; Tildesley, D. J. *Computer Simulation of Liquids*; Clarendon Press: Oxford, U.K., 1987.

(32) Berendsen, H. J. C.; Postma, J. P. M.; van Gunsteren, A.; DiNola, A.; Haak, J. R. *J. Chem. Phys.* **1984**, *81*, 3684.

(33) Street, W. B.; Tildesley, D. J.; Saville, G. *Mol. Phys.* **1978**, *35*, 639.

(34) Breneman, C. P.; Wiberg, K. B. *J. Comput. Chem.* **1990**, *11*, 361.

(35) Schmidt, M. W.; Baldridge, K. K.; Boatz, J. A.; Elbert, S. T.; Gordon, M. S.; Jensen, J. J.; Koseki, S.; Matsunaga, N.; Nguyen, K. A.; Su, S.; Windus, T. L.; Dupuis, M.; Montgomery, J. A. *J. Comput. Chem.* **1993**, *14*, 1347.

(36) DL_POLY is a parallel molecular dynamics simulation package developed at the Daresbury Laboratory Project for Computer Simulation under the auspices of the EPSRC for the Collaborative Computational Project for Computer Simulation of Condensed Phases (CCP5) and the Advanced Research Computing Group (ARCG) at the Daresbury Laboratory.

(37) Jorgensen, W. L.; Gao, J. *J. Phys. Chem.* **1986**, *90*, 2174.

(38) Pearlman, D. A.; Kollman, P. A. *J. Chem. Phys.* **1991**, *94*, 4532.

(39) Boyd, R. H. *J. Chem. Phys.* **1969**, *51*, 1470.

(40) Aue, D. H.; Webb, H.; Webb, M.; Bowers, M. T. *J. Am. Chem. Soc.* **1976**, *98*, 318.

(41) Chandra, A.; Chowdhuri, S. *J. Phys. Chem. B* **2002**, *106*, 6779.

(42) Chandra, A. *J. Phys. Chem. B* **2003**, *107*, 3899.